Available online at www.sciencedirect.com
ScienceDirect
Journal of the European Ceramic Society 32 (2012) 299–306
www.elsevier.com/locate/jeurceramsoc

Structural characterization of bulk $ZrTiO_4$ and its potential for thermal shock applications

E. López-López [a], C. Baudín [a,*], R. Moreno [a], I. Santacruz [b], L. Leon-Reina [c], M.A.G. Aranda [b]

[a] *Instituto de Cerámica y Vidrio (CSIC), C/Kelsen 5, 28049 Madrid, Spain*
[b] *Departamento de Química Inorgánica, Cristalografía y Mineralogía, Universidad de Málaga, 29071 Málaga, Spain*
[c] *Servicios Centrales de Investigación, Universidad de Málaga, 29071 Málaga, Spain*

Received 1 June 2011; received in revised form 1 August 2011; accepted 4 August 2011
Available online 7 September 2011

Abstract

Zirconium titanate, $ZrTiO_4$, is a well known compound in the field of electroceramics. Furthermore, it shows a large potential as structural material for thermal shock resistance applications, since it presents crystallographic anisotropy in thermal expansion. However, there is no information in the current literature about its thermomechanical behaviour. In this work, single phase zirconium titanate bulk materials have been prepared from well dispersed ZrO_2 and TiO_2 mixed suspensions, combining reaction and conventional sintering processes. The crystal structures of $ZrTiO_4$ have been studied by the Rietveld method for bulk samples. The structural evolution upon the cooling rate has been unravel, as the *b*-axis strongly decreases for slow cooled samples when compared to quenched materials. For the first time apparent Young's modulus (≈130 GPa) and Vickers hardness (≈8 GPa) values of a fully dense single phase zirconium titanate material have been evaluated and its potential for thermal shock applications has been analysed in comparison with other thermal shock resistant materials.

Keywords: A. Suspensions; B. X-ray methods; C. Mechanical properties; D. Zirconium titanate; E. Structural applications

1. Introduction

In general, compounds displaying anisotropic thermal expansion are good candidates to form low thermal expansion materials,[1] which are frequently used in the field of structural applications involving thermal shocks.

Aluminium titanate[2,3] is one of the compounds most widely used as a constituent of low thermal expansion materials. However, aluminium titanate decomposes into Al_2O_3 and TiO_2 at temperatures between 1073 and 1553 K, typical range of temperatures where oxides are used for structural applications. Moreover, low thermal expansion of aluminium titanate materials is always associated to extremely low values of fracture strength (≈20 MPa at 298 K).[4] For these reasons, it is necessary to search other compounds with crystallographic anisotropy in thermal expansion to overcome the current limitations of the available materials and to enlarge the range of thermal shock resistant ceramics.

Zirconium titanate, $ZrTiO_4$, is a well known compound in the field of electroceramics, where it has been used in dielectric resonators and materials for telecommunications.[5–10] In spite of its large potential as structural material for thermal shock resistance applications, since it shows anisotropic thermal expansion ($\alpha_{a298-1073K} = 8.0 \times 10^{-6}\,K^{-1}$, $\alpha_{b298-1073K} = 10.0 \times 10^{-6}\,K^{-1}$, $\alpha_{c298-1073K} = 6.2 \times 10^{-6}\,K^{-1}$, P*bcn* setting),[11] there is no information in the current literature about its thermomechanical behaviour. In particular, it is not known whether its crystalline thermal expansion anisotropy will originate sufficient thermal stresses in $ZrTiO_4$ bulk materials as to develop microcracked microstructures as occurs in the typical low thermal expansion thermal shock resistant materials.

Zirconium titanate is an intermediate compound in the binary system ZrO_2–TiO_2.[12–14] Several authors have studied this system to establish the equilibrium phases.[13,15,16] McHale and Roth heated samples of $ZrTiO_4$ at $T \approx 1273$ K around 4 months and they concluded that the stable compound of the binary system ZrO_2–TiO_2 at room temperature was $ZrTi_2O_6$.[15] Other authors

* Corresponding author.
E-mail address: cbaudin@icv.csic.es (C. Baudín).

0955-2219/$ – see front matter © 2011 Elsevier Ltd. All rights reserved.
doi:10.1016/j.jeurceramsoc.2011.08.004

studied the influence of cooling rate in the lattice parameters of zirconium titanate at room temperature.[5,11,13,17,18] Some authors proposed two phases to explain the differences in lattice parameters due to different cooling rates.[13,18] However, other study[19] reported an important change in the *b* lattice parameter (P*bcn* setting) as function of the cooling rate, after sintering, that it was assigned to local ordering of the Ti, Zr-cations for slow cooling treatments.

The synthesis of $ZrTiO_4$ has been reported by several methods including sol-gel,[8,20–23] co-precipitation,[24,25] mechanochemical processing[26] and solid state reaction.[12,13,15,16,27] These methods have been used to make powders or small pieces of $ZrTiO_4$. However, structural applications require bulk materials, so it is necessary to combine synthesis and processing methods which allow the preparation of zirconium titanate 3D-shaped materials.[28,29]

This work deals with the fabrication of single phase $ZrTiO_4$ bulk materials by solid state reaction of ZrO_2 and TiO_2. The final goal is to determine the basic thermomechanical properties to evaluate the true possibilities of $ZrTiO_4$ as a constituent of thermal shock resistance materials. In order to do so, the Vickers hardness and the apparent Young's modulus values of isostatic pressed bodies sintered at 1773 K for 12 h are reported and discussed.

2. Experimental

Commercial m-ZrO_2 (TZ-0, Tosoh Tokyo, Japan) and anatase-TiO_2 (808, Merck, Darmstadt, Germany) were used as starting powders. Both powders have average particle diameters of 0.3 μm and the specific surface areas are 14 m^2/g for m-ZrO_2 and 9 m^2/g for TiO_2.

Particle size distribution was determined with a laser diffraction analyser (Mastersizer S, Malvern, Worcestershire, UK), and the specific surface area was measured by the N_2 adsorption method (Monosorb Surface Area Analyzer MS13, Quantachrome Co., Boynton Beach, Florida, USA). Colloidal stability of m-ZrO_2 (Z) and TiO_2 (T) suspensions was determined through zeta potential measurements by the laser Doppler electrophoresis technique (Zetasizer NanoZS, Malvern, Worcestershire, UK). Suspensions were prepared to a solids content of 0.01 wt.% by mixing with an ultrasonic probe (UP 400 S, Hielscher, Stuttgart, Germany) for 2 min in a solution of KCl 10^{-2} M to maintain a constant ionic strength. Slurries were stirred for 20 h prior to measurements in order to reach surface equilibrium. A polyacrylic-based dispersant (Dolapix CE64, Zschimmer-Schwarz, Lahnstein, Germany) was used as the dispersing aid. The influence of the polyelectrolyte concentration on the zeta potential was also investigated. Concentrated aqueous suspensions of m-ZrO_2 (Z) and TiO_2 (T) were prepared separately. Solid contents were 40 vol.% (≈80 wt.%) for Z and 45 vol.% (≈76 wt.%) for T. Both slurries were prepared by adding the powder to the proper amount of deionised water containing polyacrylic-based dispersant (Dolapix CE64) to a total concentration of 0.8 wt.% on a dry solids basis, and further mixing with a high shear mixer (L2R, Silverson, Chesham, UK). Then, they were ball milled for 24 h using alumina jar and balls. The as-prepared one component slurries were mixed to relative molar ratio of 1 in order to obtain Z + T suspension. The resulting mixture was ball milled during one additional hour to assure uniform mixing. Details of the preparation procedure are given in a previous work.[28]

For rheological characterisation of the suspensions a rotational rheometer (RS50 Thermo, Thermo-Haake, Karlsruhe, Germany) with a double cone/plate geometry was used. Flow curves were performed by changing shear rate between 0 and 1000 s^{-1} for 5 min for the up and down ramps. Dwell time at the maximum rate was 1 min. Temperature was maintained constant at 298 K. All suspensions were prepared and measured at least three times and representative curves are given.

Z + T green bodies were shaped into plates (≈70 mm × 70 mm × 10 mm) by slip casting the Z + T suspension in plaster moulds and dried in air for 48 h. Green and sintered densities were determined by Archimedes' method, using mercury and deionised water, respectively. Open porosity was determined in sintered samples immersing samples in boiled deionised water and heating it up to boiling point during 2 h.

Constant heating rate (CHR, heating and cooling rates 5 K/min) experiments up to 1973 K were performed in a differential dilatometer with alumina rod (DI24, Adamel Lhomargy, Brie, France). From the derivatives of the shrinkage-temperature curves two temperatures (1210 and 1450 K) were selected to prepare quenched specimens to determine the crystalline phases present at both temperatures during the reaction sintering process. The experimental procedure to obtain the quenched specimens consisted in heating at 5 K/min to the final temperature (dwell time 1 min) in an electrical furnace, and quenching in air stream using an electric fan. This cooling method assures cooling times from the treatment temperature to 1073 K of less than 1 min for the small (≈5 mm × 5 mm × 5 mm) specimens used. From the phase analysis of the quenched specimens and the shrinkage curves, the selected temperature to sinter Z + T green compacts was 1773 K. Higher temperatures were observed to lead to liquid formation in the material. Specimens were fabricated by treating the green compacts at 1773 K using different dwell times (2, 8 and 12 h).

Since it was not possible to get dense materials directly by the single-step reaction sintering process described above, conventional sintering of green compacts of already reacted ZT powders was investigated. ZT specimens were obtained after sintering the Z + T green compacts at 1773 K for 2 h, attrition milling (Y_2O_3-stabilized ZrO_2, diameter 3 mm: YTZ Grinding Media, Tosoh Co, Tokyo, Japan) the sintered compacts during 4 h, drying and sieving the resulting powder using 37 μm mesh diameter, further compactation of the sieved powders by isostatic pressing at 200 MPa and finally sintering the ZT pressed compacts at 1773 K during 12 h. Conventional sintering process was performed with heating rate of 5 K/min and cooling rate of 5 K/min to 1373 K and then 2 K/min to room temperature.

Quenched specimens were characterised as pieces by X-ray diffraction (XRD) (D8 Advance, Bruker, Karlsruhe, Germany). The obtained XRD patterns were analysed using the diffraction files of $ZrTiO_4$ (PDF: 00-034-0415), a-TiO_2 (PDF:

00-021-1272), r-TiO_2 (PDF: 00-021-1276), m-ZrO_2 (PDF: 00-037-1484) and t-ZrO_2 (PDF: 01-079-1770).

To investigate the role of the cooling rate on the crystal structure of $ZrTiO_4$ bulk samples, three specimens were prepared as described above (heating at 1773 K during 12 h) and cooled at different rates, particularly in the temperature range between 1473 and 1373 K, which is the temperature range where some authors reported important changes in the cell parameters.[18,30] ZT-q stands for the sample heated at 1773 K/12 h and quenched from 1773 K to room temperature as previously explained. ZT-5 stands for the sample heated at 1773 K/12 h and cooled at 5 K/min from 1773 K to 1373 K, and then, at 2 K/min from 1373 K to room temperature (20 min was the total time at temperatures 1373–1273 K). Finally, ZT-sc (the slow cooled sample) stands for the sample heated at 1773 K/12 h and cooled at 5 K/min from 1773 K to 1473 K, at 0.1 K/min 1473–1373 K, and then at 2 K/min to room temperature (1000 min was the total time at temperatures 1473–1373 K).

X-ray diffraction patterns for the three specimens (ZT-q, ZT-5 and ZT-sc) were recorded on a PANalytical X'Pert PRO MPD diffractometer working in reflection geometry ($\theta/2\theta$) and using the X'Celerator RTMS (Real Time Multiple Strip) detector with an active length of 2.122°. The compact flat specimens were loaded in a multi-purpose sample holder which allows the micrometric controlled alignment of samples with a mass up to 1 kg. The patterns were collected with a long fine focus Cu tube working at 45 kV and 40 mA. The incident beam optic path contained a hybrid monochromator (composed of a W/Si parabolic X-ray graded mirror and a flat Ge (220) asymmetric monochromator) which yielded a strictly monochromatic, $\lambda = 1.54059$ Å parallel X-ray beam, and a fixed 1/8° anti-scatter slit. The diffracted beam optic path contained a fixed 1/8° divergence slit. Both, incident and diffracted beams were equipped with 0.02 rad Soller slits. A typical scan range was from 20.0 to 100.0° 2θ with a step size of 0.0167° 2θ and an overall recording time of approximately 4 h. The patterns were analysed by the Rietveld method[31] using the GSAS program.[32]

The microstructure of diamond polished (down to 3 μm) samples was characterized by scanning electron microscopy (TM-1000 Tabletop, Hitachi, Tokyo, Japan).

Pieces (≈10 mm × 10 mm × 5 mm) machined from the sintered blocks were tested in a differential dilatometer (402 EP, Netzsch, Selb, Germany) to obtain the thermal expansion curves from tests with heating and cooling rates of 2 K/min. The average thermal expansion coefficient between room temperature and 1123 K for ZT material was calculated from the curves. The reported result is the average of three determinations and error is the standard deviation of these measurements.

Instrumented indentation tests were performed using a specially developed electromechanical indentation device (Microtest, Madrid, Spain).[33] The indenter is a diamond Vickers pyramid with angle of 136°. Loading was performed in displacement control at a constant rate (0.05 mm/min) up to 100 N. Then, the load was held for 10 s, and finally, unloading was performed at the same rate. Apparent Young's modulus was calculated using the Oliver and Pharr model.[34,35] Vickers hardness was calculated using Eq. (1), where P is the maximum load and a is the length of the semidiagonal of the residual impression measured by optical microscopy (H-P1, Carl-Zeiss, Oberkochen, Germany) with an accuracy of ±3 μm.

$$H_v = 0.4636 \cdot \frac{P}{a^2} \quad (1)$$

Additionally, apparent Young's modulus was also determined by instrumented indentation for mullite specimens fabricated by conventional sintering of commercial powders (grain size ≈1 μm[36] and theoretical density ≈97%[37]) for comparison purposes.

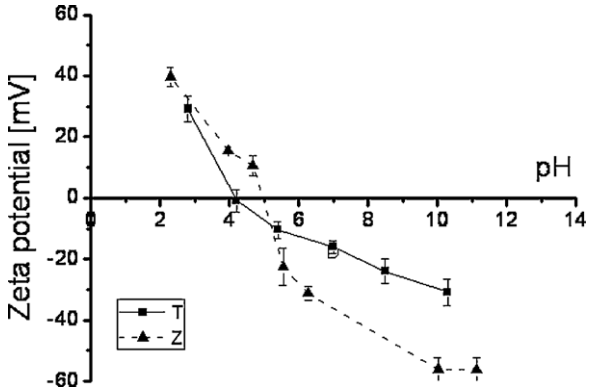

Fig. 1. Zeta potential of the powders used in this work as a function of pH.

3. Results and discussion

3.1. Processing

Fig. 1 shows the evolution of zeta potential of the powders used in this work as a function of pH. Isoelectric point values were ≈5.0 and ≈4.2 for Z and T, respectively. It can be observed that the highest values of zeta potential are generated at extreme pH values in both cases. So, in order to get stable slurries, it is necessary to add a dispersant to avoid working at such extreme pH values. In this sense the use of a polyelectrolyte (Dolapix CE64) provides an electrosteric stabilizing mechanism and allows working at moderate pH values.

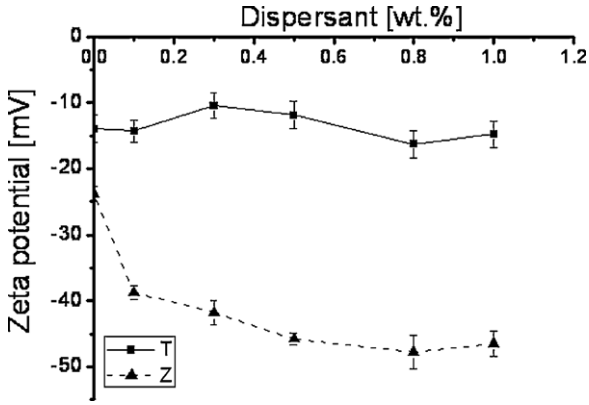

Fig. 2. Zeta potential of the powders used in this work as a function of dispersant content.

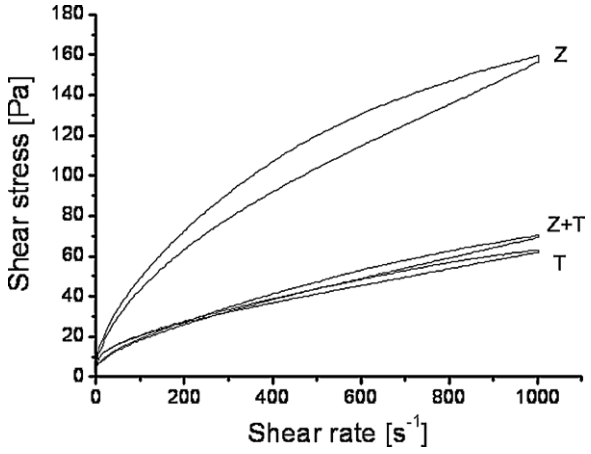

Fig. 3. Flow curves of Z, T and Z + T concentrated suspensions.

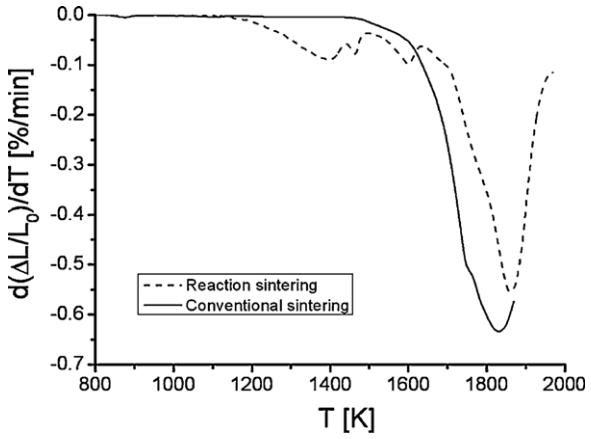

Fig. 4. Derivative of dilatometry curves versus temperature during heating (constant heating rate) for Z + T (dash line) and ZT (solid line) green compacts.

Fig. 2 shows the evolution of zeta potential as a function of dispersant content. It can be observed that the optimum amount of dispersant to reach the highest zeta potential for Z is 0.8 wt.%. Although no significant variation was observed for T, 0.8 wt.% was selected as the optimum to avoid competitive adsorption in the subsequent Z + T suspension.

Fig. 3 shows the flow curves of Z, T and Z + T concentrated suspensions. It can be observed that T suspension presents viscosity values lower than Z suspension and lower thixotropy. The rheological behaviour of Z + T suspension is closer to that of the T suspension. So, the presence of TiO_2 controls the rheological behaviour of the Z + T mixtures.

Fig. 4 shows the results of constant heating rate (CHR) experiments for Z + T and ZT green compacts. From the derivative curve for Z + T, the selected temperature for isothermal reaction sintering process was 1773 K. Although the maximum shrinkage rate occurs at about 1873 K, liquids were observed to form in materials sintered at temperatures higher than 1773 K. Thus, several dwell times at 1773 K were tested in order to achieve the highest density.

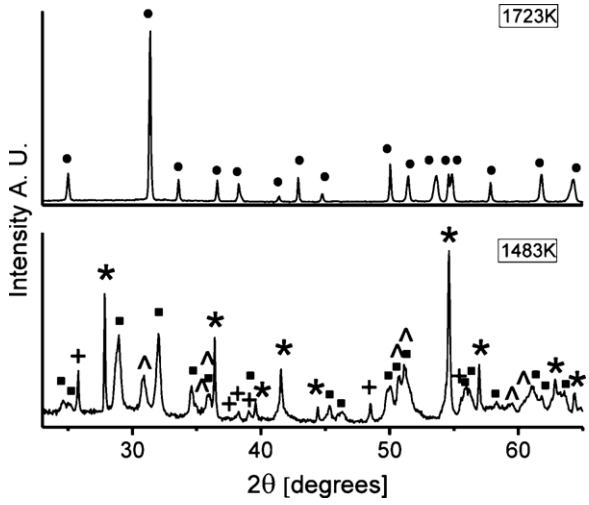

Fig. 5. X-ray diffraction pattern of ZT green compacts after quenching tests in air from the indicated temperatures, 1483 and 1723 K. (●) $ZrTiO_4$, (*) r-TiO_2, (+) a-TiO_2, (■) m-ZrO_2, (^) t-ZrO_2. It can be observed there is still not reaction of formation of ZrTiO4 at 1483 K, coexisting a mixture of r-TiO_2, a-TiO_2, m-ZrO_2 and t-ZrO_2, whereas $ZrTiO_4$ is the only phase present at 1723 K.

Table 1 shows relative density and open porosity values for the specimens sintered at 1773 K/12 h. For the reaction sintered material, Z + T, the density reached is extremely low and, moreover, the material shows high open porosity as corresponds to initial sintering stages. In order to investigate the reason for such behaviour, the processes involved during reaction sintering of Z + T green compacts were investigated. Fig. 5 shows the XRD patterns of Z + T compacts heated to 1483 and 1723 K and quenched. The major phase of TiO_2 at 1483 K is rutile, although there is some anatase still remaining, meanwhile ZrO_2 appears as m-ZrO_2 (major phase) and t-ZrO_2. The material quenched from 1723 K shows the typical pattern of $ZrTiO_4$. This fact indicates that complete formation of $ZrTiO_4$ occurs at temperatures lower than 1723 K.[29] The formation of $ZrTiO_4$ arrests the initiation of shrinkage of the compact as observed in the shrinkage-temperature curve (see Fig. 4).

The above discussion demonstrates that for the submicron powders used in this work, it is not possible to obtain a fully dense ZT material by reaction sintering because reaction occurs at temperatures lower than that required for shrinkage, arresting it. This makes necessary to promote the reaction to obtain $ZrTiO_4$, which is then subjected to attrition milling, sieving,

Table 1
Characteristics of the green and sintered compacts. Data for sintered materials correspond to those that presented the lowest open porosity values for each processing route. Z + T: $ZrO_2/TiO_2 = 1$ (mol); ZT = $ZrTiO_4$.

Green compact	Green density (g/cm^3)	Relative density (%)	Shaping procedure	Thermal treatment	Relative sintered density (%)	Open porosity (%)
Z + T	2.6 ± 0.1	54 ± 1	Slip casting	1773 K/12 h	84 ± 1	9 ± 2
ZT	3.1 ± 0.1	62 ± 1	Isostatic pressing	1773 K/12 h	91 ± 1	3 ± 1

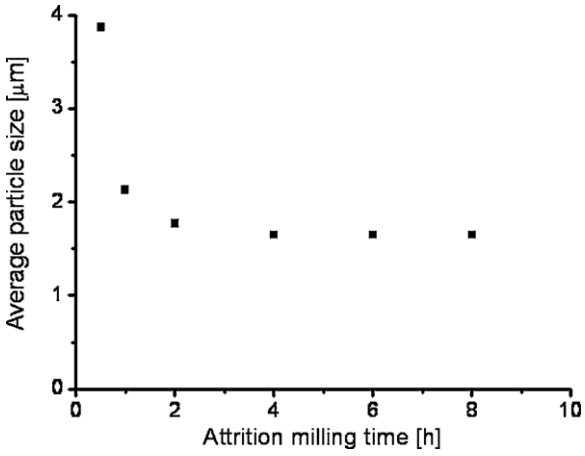

Fig. 6. Average particle size versus attrition milling time of ZT sintered material.

isostatic pressing and further conventional sintering processes. These processes were done using Z + T compacts treated at 1723 K during 2 h which were fully reacted and presented high porosity (≈22%) that facilitated milling.

To obtain fine powders free of aggregates, milling has to be adequately controlled. Fig. 6 shows the variation of the average particle size versus attrition milling time of the ZT compacts. 4 h was selected as the optimum milling time since further milling did not lead to smaller particle sizes.

Fig. 4 also shows the shrinkage-temperature curve for the ZT green compact. Maximum shrinkage rates are reached at lower temperature (≈1833 K) than for the reaction sintered compact. As it was not possible to use temperatures higher than 1773 K to avoid liquid formation, after testing different dwell times at 1773 K, 12 h was selected as dwell time.

The relative density and open porosity values for the ZT compact formed by isostatic pressing of the milled powder and conventional sintering at 1773 K/12 h are also shown in Table 1. It can be observed that the relative sintered density is higher and the open porosity lower than for the reaction sintered material.

Fig. 7 shows the microstructure of the ZT material sintered at 1773 K/12 h. The aspect of the elongated pores would correspond to the measured open porosity (≈3%, Table 1). The presence of microcracks, which are typical in materials with crystallographic anisotropy in thermal expansion, such as $AlTiO_4$, is not detected.

3.2. Crystal structure and phase analysis

The laboratory X-ray powder diffraction characterisation of the studied $ZrTiO_4$ materials, ZT-q (quenched from 1773 K to room temperature), ZT-5 (cooled at 5 K/min from 1473 to 1373 K) and ZT-sc (cooled at 0.1 K/min from 1473 to 1373 K), shows that they are highly crystalline single phases. $ZrTiO_4$ crystallizes in a cation-disordered P*bcn* orthorhombic α-PbO_2 type structure.[38] However, as pointed out previously[19] the *b*-axis parameter varies strongly with the cooling rate. This behaviour is highlighted in Fig. 8 where a selected region of the XRD patterns of ZT-q, ZT-5 and ZT-sc are given. Due to the *b*-axis variation with the cooling rate, the (2 0 0) and (0 2 1) reflections are fully

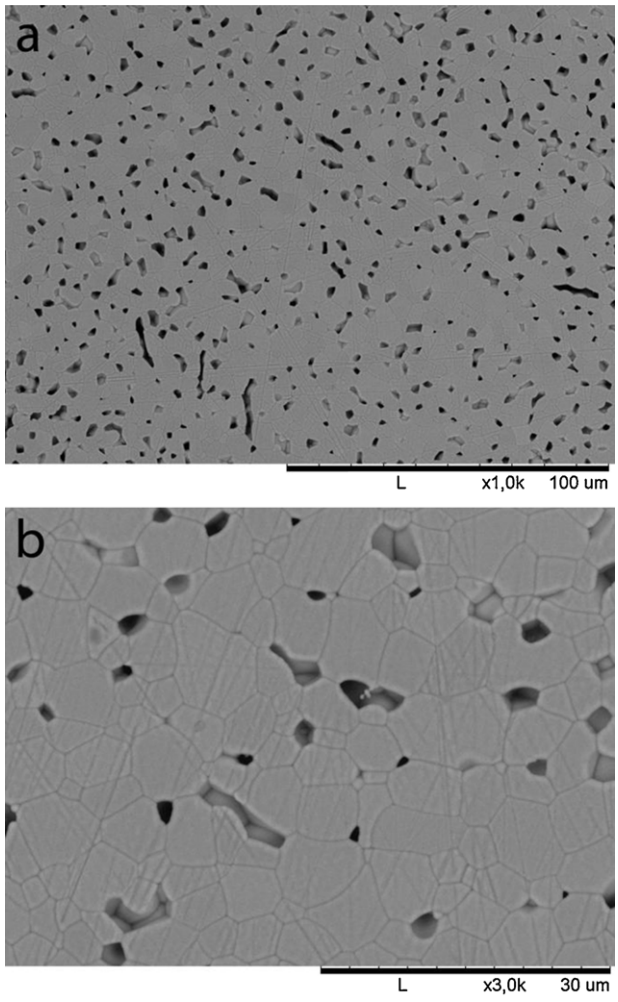

Fig. 7. Microstructure of the ZT material sintered at 1500 °C/12 h. SEM micrographs of polished and thermally etched (1400 °C/1 min) surfaces.

overlapped for ZT-q but totally resolved for ZT-sc. These reflections are partially overlapped for intermediated cooling rates, as expected, see ZT-5 pattern in Fig. 8.

To better understand the structural evolution of $ZrTiO_4$ with the cooling rate, full Rietveld fits were carried out for the three patterns. As an example, the diffraction fit for ZT-q sample is given in Fig. 9. This figure also contains an enlarged view of the fit to the high angle region to highlight the high quality of the analysis. The final structural results are given in Table 2. The influence of the cooling rate on the unit cell parameters is profound as the unit cell volume shrinks for low cooling rates. This thermal behaviour is not isotropic, as *c*-axis does not depend upon the cooling rate but *a*-axis slightly increases for low rates and *b*-axis strongly decreases for slow cooling when compared to quenched materials.

In order to understand the unit cell dependence, at room temperature, with the cooling rates for $ZrTiO_4$ single phase samples, full structural refinements were carried out, see Table 2. The refined positional parameter for the metal also shows a clear trend with the cooling rate. As it can be seen in Table 2, y_M decreases from 0.301 for the quenched sample to 0.294 to the slowly cooled sampled. As the crystal structures have

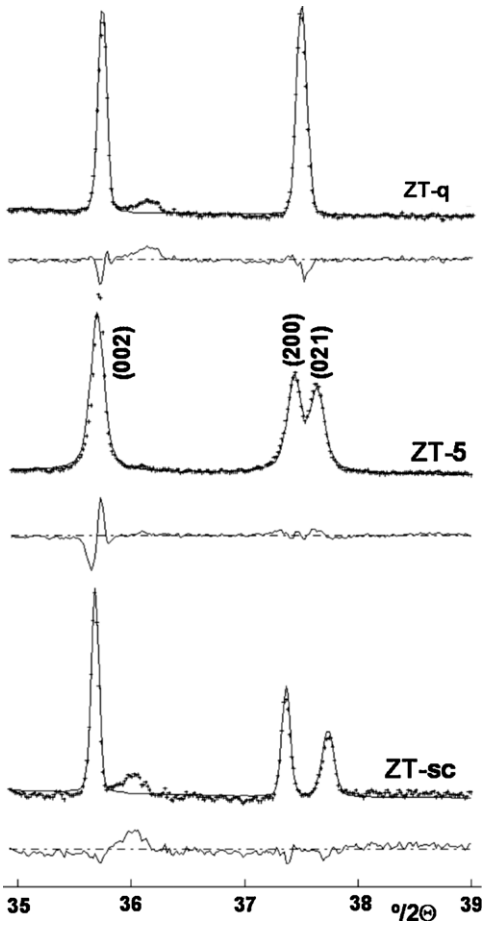

Fig. 8. Selected region of the laboratory X-ray piece diffraction patterns for the $ZrTiO_4$ samples prepared at different cooling rates, see experimental section, showing the good fit with the α-PbO_2 type structure but highlighting the overlapping consequences of the *b*-axis variation.

Table 2
Selected structural results for $ZrTiO_4$ samples prepared ad different cooling rates, ZT-q, ZT-5 and ZT-sc (space group P*bcn*).

	ZT-q	ZT-5	ZT-sc
a/Å	4.8060(1)	4.8101(1)	4.8156(1)
b/Å	5.4773(1)	5.4389(1)	5.4174(1)
c/Å	5.0332(1)	5.0337(1)	5.0332(1)
V/Å^3	132.49(1)	131.69(1)	131.31(1)
Calculated density/g/cm^3	5.09	5.12	5.14
R_{WP}/%	6.6	9.2	5.1
R_F/%	6.5	6.2	8.7
y[a] (M)	0.3007(2)	0.2957(1)	0.2944(2)
x (O)	0.2704(8)	0.2701(7)	0.2676(9)
y (O)	0.0995(6)	0.1017(6)	0.0936(8)
z (O)	0.0672(7)	0.0600(6)	0.0626(8)

[a] In this crystal structure, Zr/Ti are randomly located at the special position (1/2 and 1/4).

been refined, the bond distances and angles can be calculated. The average octahedral M–O distances are 2.043, 2.045 and 2.046 Å, for ZT-q, ZT-5 and ZT-sc, respectively. The variation of the atomic parameters and the average metal–oxygen distances are compatible with a partial (local) metal ordering for slowly cooled materials, in agreement with previous electron microscopy results.[19] However, neutron powder diffraction would be needed to precisely measure the oxide position change with the cooling rate.

Finally, it must be noted that the structural results reported here are obtained for compact specimens, i.e. not loose powders. This is important for two reasons. Firstly, the grinding step is avoided which may introduce structural imperfections that complicate the analysis and may affect the results. Secondly, and more importantly, the structure of the materials is studied in the conditions of compaction and densification where they will be used for thermal shock resistance applications.

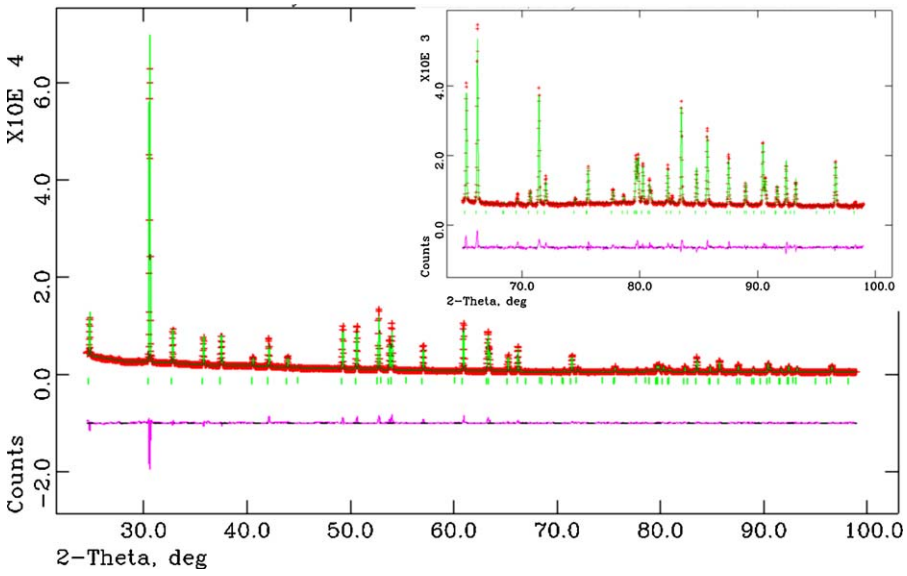

Fig. 9. Observed (crossed), calculated (full line) and difference curve (bottom) X-ray powder diffraction profiles for single phase $ZrTiO_4$ material quenched, obtained by Rietveld refinement using the GSAS software. The vertical marks show the diffraction peak positions allowed by the P*bcn* space group. The high-quality of the fit is apparent by the coincidence between the observed and calculated curves, highlighted by the insert enlarges in the high angle region.

Table 3
Average thermal expansion coefficient between 298 and 1123 K ($\alpha_{298–1123}$), Vickers hardness (H_v) and apparent[a] (E_{app}) values of ZT sintered material.

	$\alpha_{298–1123\ K}$ (K^{-1})	H_v (GPa)	E_{app} (GPa)
ZT	$8.1 \pm 0.2 \times 10^{-6}$	6.1 ± 0.3	99 ± 6

[a]Calculated from the unload portion of the instrumented indentation curves.

3.3. Properties

As discussed above, the ZT material sintered at 1773 K during 12 h and cooled using a characteristic cooling schedule for ceramics, ZT-5, was fully constituted by $ZrTiO_4$. Thus, such material was adequate to determine the basic properties involved in thermal shock resistance: Young's modulus and thermal expansion coefficient. Additionally, hardness was determined to evaluate its structural integrity. These properties have not been reported in the literature.

Table 3 shows the thermal expansion coefficient, Vickers hardness and apparent Young's modulus values of ZT sintered material. The average thermal expansion coefficient between room temperature and 1123 K ($\alpha_{298–1123}$) was calculated from dilatometric curves which did not present hysteresis, as corresponds to the absence of microcracks. The obtained value is similar to the average crystallographic thermal expansion coefficient value calculated from data reported by Ikawa et al.[11] discussed in the introduction of this work. Such similarity further demonstrates the lack of microcracks in this material.

It is possible to calculate the properties values for a fully dense material (zero porosity) using Eqs. (2) and (3).[39,40]

$$E = E_0 e^{(-bP)} \quad (2)$$

$$H = H_0 e^{(-bP)} \quad (3)$$

E_0 and H_0 are Young's modulus and Vickers hardness values of a fully dense material, respectively. P is the volume fraction of porosity and b is a constant which depends on pore shape and Poisson's ratio and it can be determined from experimental results by data fitting.

Assuming spherical shape for the pores in the ZT material and a Poisson's ratio similar to that of alumina, the b value will be 3;[39] spherical pores are characteristic of closed porosity and Poisson's ratio values of dense ceramics are similar and in the range 0.2–0.3. Using data from Table 3, E_0 and H_0 values would be ≈130 GPa and ≈8 GPa, respectively. The calculated Vickers hardness value indicates that a fully dense single phase $ZrTiO_4$ material would have hardness values similar to those of other ceramic oxides. The calculated Young's modulus value is lower than that of other crack-free ceramic materials used for thermal shock resistance, such as mullite ceramics (Table 4).

According to the thermoelastic theory, the lower is the value of the product between α and E, the more resistant to thermal shock will be the material. In this sense Table 4 shows E, α and $E{\cdot}\alpha$ values of a fully dense single phase $ZrTiO_4$ material compared to those reported for the fully dense reference mullite material and for aluminium titanate materials.[4,41,42] It can be observed that aluminium titanate presents the lowest $E{\cdot}\alpha$ value. The extremely high crystallographic anisotropy in thermal expansion is responsible for cracking of aluminium titanate materials with relatively small grain sizes (≈1 μm).[43] On the contrary, the thermal stresses associated to the crystallographic anisotropy in thermal expansion of $ZrTiO_4$ are not enough to develop cracks in the studied monophase material, thus, it cannot be included in the category of low thermal expansion thermal shock resistant materials. Therefore, the developed $ZrTiO_4$ material is compared to an uncracked mullite material, a typical thermal shock resistance oxide. Data in Table 4 show that $E{\cdot}\alpha$ values are quite similar, suggesting the potential of $ZrTiO_4$-based materials for thermal shock.

Table 4
Average thermal expansion coefficient (α), Young's modulus (E) and $E{\cdot}\alpha$ values of ZT sintered material, mullite and aluminium titanate (Al_2TiO_5).

	α (K^{-1})	E (GPa)	$E{\cdot}\alpha$ (MPa K^{-1})
ZT ($ZrTiO_4$)	$8.1 \pm 0.2 \times 10^{-6}$	≈130[a]	≈1.1
Mullite	$4.1 \pm 0.1 \times 10^{-6}$ [36]	159 ± 25[b]	0.7 ± 0.2
Al_2TiO_5	$\approx 1.0–1.7 \times 10^{-6}$ [4,41]	≈10–20[4,41,42]	≈0.01–0.03

[a]Calculated using apparent Young's modulus value (Table 3) and Eq. (2).
[b]Calculated from the unload portion of the instrumented indentation curves.

4. Conclusions

This work reports the manufacture of single-phase, dense $ZrTiO_4$ bulk materials according to a two-steps processing schedule consisting in the shaping and reaction sintering of ZrO_2 and TiO_2 to form $ZrTiO_4$ and its further milling, isopressing and conventional sintering using cycles typical for ceramics.

The crystal structures of $ZrTiO_4$ belong to the α-PbO_2 type structure but its fine details depend upon the cooling rate. The structural characterisation by X-ray diffraction has been carried out on dense bulk specimens and the positional atomic parameter variations are compatible with partial short-range order of Zr/Ti metals.

To the best of our knowledge there is no literature reporting any thermomechanical properties of single phase $ZrTiO_4$ materials. The level the residual stresses that would be developed in such materials, evaluated from the experimental Young's modulus and average thermal expansion coefficient of the developed material, are higher than those for in a typical low thermal expansion microcracked oxide (aluminium titanate) and in the range of those for a typical low thermal expansion uncracked one (mullite). This latter result suggest that $ZrTiO_4$-based materials are candidates for thermal shock applications.

Acknowledgments

The work in Madrid has been supported by Spanish Ministry of Science and Innovation under contract MAT2009-14369-C02-01. E. López-López acknowledges to Community of Madrid (Spain) and European Social Fund for economical support by CPI/0552/2007 contract. The work in Malaga has been supported by the research grant FQM-113 from Junta de

Andalucía, Spain and Spanish Ministry of Science and Innovation through a Ramón y Cajal fellowship (RYC-2008-03523).

References

1. Roy R, Agrawal DK, McKinstry HA. *Very low thermal expansion coefficient materials*. *Annu Rev Mater Sci* 1989;**19**:59–81.
2. Morishima H, Kato Z, Uematsu K, Saito K, Yano T, Ootsuka K. *Synthesis of aluminium titanate–mullite composite having high thermal shock resistance*. *J Mater Sci Lett* 1987;**6**:389–90.
3. Morishima H, Kato Z, Uematsu K, Saito K. *Development of aluminium titanate–mullite composite having high thermal shock resistance*. *J Am Ceram Soc* 1986;**69**:C-226–7.
4. Milosevski M, Ondracek O, Milisevska R, Spaseska D, Dimeska A. *Thermal expansion and mechanical properties of Al_2TiO_5–SiO_2 system*. *Adv Sci Technol* 1995:1875–82.
5. Park Y, Kim Y. *Influence on cooling rate on the physical properties of tin modified zirconium titanate*. *J Mater Sci Lett* 1996;**15**:853–5.
6. Wolfram G, Göbel HE. *Existence range, structural and dielectric properties of $Zr_xTi_ySn_zO_4$ ceramics ($X + Y + Z = 2$)*. *Mater Res Bull* 1981;**16**: 1455–63.
7. Bianco A, Gusmano G, Freer R, Smith P. *Zirconium titanate microwave dielectrics prepared via polymeric precursor route*. *J Eur Ceram Soc* 1999;**19**:959–63.
8. Hirano S, Hayashi T, Hattori A. *Chemical processing and mircrowave characteristic of (Zr, Sn)TiO_4 microwave dielectrics*. *J Am Ceram Soc* 1991;**74**:1320–4.
9. Christoffersen R, Davies PK, Wei X, Negas T. *Effect of Sn substitution on cation ordering in $(Zr_{1-x}Sn_x)TiO_4$ microwave dielectric ceramics*. *J Am Ceram Soc* 1994;**77**:441–50.
10. Victor P, Bhattacharyya S, Krupanidhi SB. *Dielectric relaxation in laser ablated polycrystalline $ZrTiO_4$ thin films*. *J Appl Phys* 2003;**94**: 5135–42.
11. Ikawa H, Iwai A, Hiruta K, Shimojima H, Urabe K, Udagawa S. *Phase transformation and thermal expansion of zirconium and hafnium titanates and their solid solutions*. *J Am Ceram Soc* 1988;**71**:120–7.
12. Brown FH, Duwez P. *The zirconia–titania system*. *J Am Ceram Soc* 1954;**37**:129–32.
13. Coughanour LW, Roth RS, DeProsse VA. *Phase equilibrium relations in the systems lime–titania and zirconia–titania*. *J Res Nat Bur Stand* 1954;**52**:37–42.
14. López-López E, Moreno R, Baudín C. *Titanato de circonio: estabilidad y expansión térmica*. *Bol Soc Esp Ceram V* 2011;**50**:169–76, doi:10.3989/cyv.222011.
15. McHale AE, Roth RS. *Low-temperature phase relationships in the system ZrO_2–TiO_2*. *J Am Ceram Soc* 1986;**69**:827–32.
16. Troitzsch U, Ellis DJ. *The ZrO_2–TiO_2 phase diagram*. *J Mater Sci* 2005;**40**:4571–7.
17. Lynch RW, Morosin B. *Thermal expansion, compressibility, and polymorphism in hafnium and zirconium titanates*. *J Am Ceram Soc* 1972;**55**:409–13.
18. Park Y. *Thermal expansion and cooling rate dependence of transition temperature in $ZrTiO_4$ single crystal*. *Mater Res Bull* 1998;**33**: 1325–9.
19. Wang CL, Lee HY, Azough F, Freer R. *The microstructure and microwave dielectric properties of zirconium titanate ceramics in the solid solution system $ZrTiO_4$–$Zr_5Ti_7O_{24}$*. *J Mater Sci* 1997;**32**:1693–701.
20. Bhattacharya AK, Mallick KK, Hartridge A, Woodhead JL. *Sol gel preparation, structure and thermal stability of crystalline zirconium titanate microspheres*. *J Mater Sci Lett* 1996;**31**:267–71.
21. Navio JA, Marchena FJ, Macias M, Sanchez-Soto PJ. *Formation of zirconium titanate powder from a sol-gel prepared reactive precursor*. *J Mater Sci* 1992;**27**:2463–7.
22. Sham EL, Aranda MAG, Farfan-Torres EM, Gottifredi JC, Martínez-Lara M, Bruque S. *Zirconium titanate from sol-gel synthesis: thermal decomposition and quantitative phase analysis*. *J Solid State Chem* 1998;**139**:225–32.
23. Cerqueira M, Nasar RS, Longo E, Leite ER, Varela JA. *Synthesis of ultrafine crystalline $Zr_xTi_{1-x}O_4$ powder by polymeric precursor method*. *Mater Lett* 1995;**22**:181–5.
24. Kudesia R, Snyder RL, Condrate RA, McHale AE. *Structural study of $Zr_{0.8}Sn_{0.2}TiO_4$*. *J Phys Chem Solids* 1993;**54**:671–84.
25. Krebs MA, Condrate RA. *A Raman spectral characterization of various crystalline mixtures in the ZrO_2–TiO_2 and HfO_2–TiO_2 system*. *J Mater Sci Lett* 1988;**7**:1327–30.
26. Gajovic A, Furic K, Music S, Djerdj I, Tonejc A, Tonejc AM, Su D, Schlogl R. *Mechanism of $ZrTiO_4$ synthesis by mechanochemical processing of TiO_2 and ZrO_2*. *J Am Ceram Soc* 2006;**89**:2196–205.
27. Hom BK, Stevens R, Woodfield BF, Boerio-Goates J, Putnam RL, Helean KB, Navrotsky A. *The thermodynamics of formation, molar heat capacity, and thermodynamic functions of $ZrTiO_4$ (cr)*. *J Chem Thermodyn* 2001;**33**:165–78.
28. López-López E, Baudín C, Moreno R. *Synthesis of zirconium titanate-based materials by colloidal filtration and reaction sintering*. *Int J Appl Ceram Technol* 2008;**5**:394–400.
29. López-López E, Sanjuán ML, Moreno R, Baudín C. *Phase evolution in reaction sintered zirconium titanate based materials*. *J Eur Ceram Soc* 2010;**30**:981–91.
30. McHale AE, Roth RS. *Investigation of the phase transition in $ZrTiO_4$ and $ZrTiO_4$–SnO_2 solid solutions*. *J Am Ceram Soc* 1983;**66**:C18–20.
31. Rietveld HM. *A profile refinement method for nuclear and magnetic structures*. *J Appl Crystallogr* 1969;**2**:65–71.
32. Larson AC, Dreele RBV. Los Alamos National Laboratory. Report No. LA-UR-86-7 48 2000.
33. Bueno S, Baudín C. *Instrumented Vickers microindetation of alumina-based materials*. *J Mater Res* 2006;**21**:161–73.
34. Oliver WC, Pharr GM. *An improved technique for determining hardness and elastic modulus using load and displacement sensing indentation experiments*. *J Mater Res* 1992;**7**:1564–83.
35. Oliver WC, Pharr GM. *Measurement of hardness and elastic modulus by instrumented indentation: advances in understanding and refinements to methodology*. *J Mater Res* 2004;**19**:3–20.
36. Burgos-Montes O, Moreno R, Baudín C. *Effect of mullite additions on the fracture mode of alumina*. *J Eur Ceram Soc* 2010;**30**:857–63.
37. Osendi MI, Baudín C. *Mechanical properties of mullite materials*. *J Eur Ceram Soc* 1996;**16**:217–24.
38. Newnham RE. *Crystal structure of $ZrTiO_4$*. *J Am Ceram Soc* 1967;**50**(4):216.
39. Rice RW. *Evaluation and extension of physical property–porosity models based on minimum solid area*. *J Mater Sci* 1996;**31**:102–18.
40. Luo J, Stevens R. *Porosity-dependence of elastic moduli and hardness of 3Y-TZP ceramics*. *Ceram Int* 1999;**25**:281–6.
41. Stingl P, Heinrich J, Huber J. Properties and application of aluminium titanate components. In: Bunk W, Hausner H, editors. *Proceedings of the 2nd international symposium on ceramic materials and components for engines*. 1986. p. 369–79.
42. Cleveland JJ, Bradt RC. *Grain size/microcracking relationships for pseudobrookites oxides*. *J Am Ceram Soc* 1978;**61**:478–81.
43. Ohya Y, Nakagawa Z. *Grain-boundary microcracking due to thermal expansion anisotropy in aluminium titanate ceramics*. *J Am Ceram Soc* 1987;**70**:C-184–6.